Comparison of Approximate Riemann Solvers

Charlotte Kong

May 2011

Department of Mathematics
University of Reading

Supervisor: Dr P Sweby

Declaration

I con rm that this is my own work, and the use of all material from other sources has been properly and fully acknowledged.

Charlotte Kong

Acknowledgements

I'd like to thank the Mathematics Department of the University of Reading for all their support. I'd like to thank my husband for patience and tea. The NERC for nancial support. Author's Toro and LeVeque for making a complicated subject more accessible. Above all I'd like to thank Dr P Sweby for his patience and support.

Contents

List of Figures

1 Introduction

When solving systems of conservation laws, either by nite di erence or nite volume techniques, it is usual to employ an approximate Riemann solver which it is hoped captures the main features of the Riemann problem solution whilst avoiding the complexity of the exact solution, even if available. Approximate solvers have developed due to the costly nature of the iterative exact schemes and the need to approximate certain areas. There are several such solvers available for this purpose, for example Roe, Osher-Solomon, HHL, HHLC, and so on. The aim of this study is to review some of the most popular approximate schemes and highlight their stengths and

2 Fluid Dynamics and the Riemann Problem

The science of fluid dynamics concerns itself with the motion of fluids, that is liquids and gases, and has a wide range of applications including traffic flow and weather predictions. The foundations of fluid dynamics are the conservation laws, specifically those of conservation of mass, momentum and energy. For the purposes of testing approximate Riemann solvers, we concern ourselves with the Euler equations, those that govern inviscid flow. This section will introduce the Euler equations and their notation, before carrying on to introduce the Riemann problem itself. Following this specific test cases will be introduced that will be used to test solvers for potential weaknesses in the schemes. All equations will be presented in their one-dimensional form only, as further dimensions are beyond the scope of this investigation.

2.1 Euler Equations

The Euler equations govern inviscid flow; a fluid that is assumed to have no viscosity. They are concerned primarily with the conservation of mass, momentum and energy and correspond to the Navier-Stokes equations with zero viscosity and heat conduction terms. The equations are written in two different forms: *conservation* form and *non-conservation* form. We need only concern ourselves with the *conservation* form for this project, which emphasise the physical interpretation of the equations as conservation laws through a control volume fixed in space. Computationally, there are advantages to expressing the governing equations in terms of conserved variables: mass density ρ, the x-velocity component u and the total energy per unit mass E. These lead to numerical methods described as *conservative methods* [20]. To begin, we state the equations in terms of the conserved variables with the assumption that quantities involved are sufficiently smooth to allow for differentiation. Later we will remove the constraint to consider solutions containing discontinuities, such as shock waves.

$$\rho_t + (\rho u)_x = 0; \tag{2.1}$$

$$(\rho u)_t + (\rho u^2 + p)_x = 0; \tag{2.2}$$

$$E_t + [u(E + p)]_x = 0: \tag{2.3}$$

Here E is the total energy per unit volume

$$E = \tfrac{1}{2}\rho V^2 + \rho e \tag{2.4}$$

where

$$\tfrac{1}{2}V^2 = \tfrac{1}{2}V \quad V = \tfrac{1}{2}u^2$$

is the *speci c kinetic energy* and e is the *speci c internal energy*. The conservation laws (2.1)-(2.3) can be expressed in compact notation by de ning a column vector U of conserved variables and the ux vector $F(U)$ in the x directions. So (2.1)-(2.3) now read

$$U_t + F(U)_x = 0; \tag{2.5}$$

with

$$U = \begin{bmatrix} \\ u \\ \\ E \end{bmatrix}; \quad F = \begin{bmatrix} u \\ u^2 + p \\ u(E + p) \end{bmatrix}, \tag{2.6}$$

The ux vector $F = F(U)$ equations are to be regarded as functions of the conserved variable vector U.

2.2 The Riemann Problem

The *Riemann problem* consists of a conservation law together with piecewise constant data having a single discontinuity. Here we will discuss the problem for a linear system, and then discuss how the Riemann problem for the Euler equations, addressing speci c problems that will be focused on during comparisons of schemes.

The initial state of the system is de ned as

$$u(x; t = 0) = \begin{cases} u_L & \text{for} \\ \end{cases}$$

made, which will be discussed further in the following section. First this subsection will consider various types of Riemann problems which will be used to test the approximate Riemann solvers.

2.3 Speci c Riemann Problems

To discuss speci c Riemann problems we must rst introduce some concepts: shocks, rarefactions and contacts. These are all types of discontinuities which we can describe using the example of tra c ow. A *shock wave* is where density increases and velocity decreases very suddenly, for example, drivers moving fast through light tra c applying their breaks suddenly. A *rarefaction wave* occurs where the uid is becoming more rare ed as the density decreases, for example, as cars move out of a congested region, they accelerate smoothly and density in turn decreases smoothly. Contact discontinuities are surfaces that separate zones of di erent density and temperature, they are in pressure equilibrium and no gas ows across. We look for speci c known problems containing the types of discontinuities mentioned in order to test the e ectiveness of the approximate Riemann solver schemes considered.

2.3.1 Sod's Shock Tube

Sod's shock tube problem [15] is a common test for the accuracy of Riemann solvers and therefore invaluable to this study. The tests consists of a one-dimensional Riemann problem with the following parameters

$$\begin{pmatrix} \rho_L \\ u_L \\ p_L \end{pmatrix} = \begin{pmatrix} 1.0 \\ 0.0 \\ 1.0 \end{pmatrix}; \quad \begin{pmatrix} \rho_R \\ u_R \\ p_R \end{pmatrix} = \begin{pmatrix} 0.125 \\ 0.0 \\ 0.1 \end{pmatrix}. \tag{2.8}$$

This problem can be described using the Euler equations for its time evolution. This leads to three characteristics describing the propagation speed of the di erent regions of the system. These are the rarefaction wave, the contact discontinuity and the shock discontinuity. Solving this numerically it gives information on how well a scheme captures and resolves shocks and contact discontinuities and how well the correct density of the rarefaction wave is reproduced. This will be used as the main test for the schemes.

2.3.2 Blast Wave

The Blast Wave Problem we use here was presented by Woodward Collela [22] and represents the pressure and ow resulting from the deposition of a large amount of energy in a small very localised volume. For the purposes of this study we will split the blast tube problem into two: left hand and right hand sides, as it is easier to nd the exact solution this way. The parameters for this equation are as follows

$$(x;0) = 1;\ p(x;0) = \begin{cases} 1000 \ if\ 0 < x < 0{:}1; \\ 0{:}1 \ if\ 0{:}1 < x < 0{:}9; \\ 100 \ if\ 0{:}9 < x < 1; \end{cases} \text{ and } u(x;0) = 0{:} \tag{2.9}$$

This is a very severe test problem, the left half containing a left rarefaction, a contact and a right shock, and the right half containing a left shock, a contact discontinuity and a right rarefaction. Walls are present at either side of the domain for this test case, so we would want to use re ecting boundary conditions. The boundary conditions will be discussed in the next section.

2.3.3 The 123 Problem

The next problem is known as the *123 problem* and was presented by Einfeld *et al.* [5], with the following parameters,

$$(x;0) = 1;\ p(x;0) = 0{:}4; \text{ and } u(x;0) = \begin{cases} 2 \ if\ x < 0{:}5; \\ 2 \ if\ x > 0{:}5{:} \end{cases} \tag{2.10}$$

The solution of this problem consists of two strong rarefactions and a trivial stationary contact discontinuity. The intermediate state pressure p is very small, close to vacuum, and this can lead to di culties in the iteration scheme to nd p numerically.

2.3.4 Other Problems

The last test is made up of right and left shocks emerging from the solution to the left and right

$$(x;0) = 5{:}99924;\ p(x;0) = \begin{cases} 460{:}894 \ if \ x < 0{:}5 \\ 46.0950 \ if \ x > 0{:}5 \end{cases};\ \text{and}\ u(x;0) = \begin{cases} 19{:}5975 \ if \ x < 0{:}5; \\ -\ 6.19633 \ if \ x > 0{:}5{:} \end{cases} \tag{2.11}$$

The solution of this represents the collision of these two strong shocks and consists of a left facing shock travelling slowly to the right, a right travelling contact discontinuity and a right travelling shock wave.

3 Godunov's Method

The original concept of ux algorithms based on exact or approximate solutions of the Riemann problem was rst developed by Godunov [6]. In this paper, Godunov introduced utilising the solution of the local Riemann problem at each cell face as the basis for determining the ux $F_{i\ \frac{1}{2}}$ in the integral form of the Euler equations

$$U_i^{n+1} = U_i^n \quad \frac{1}{x} \int_t^{t^{n+1}} (F_{i+\frac{1}{2}} \quad F_{i\ \frac{1}{2}})dt: \tag{3.1}$$

Firstly we can think of the solution U_i for i

4 Approximate Riemann Solvers

This chapter will brie y introduce some concepts needed for approximate Riemann solvers. It will also provide useful information on the structure of approximate programs, how time step size is chosen and so on.

4.1 Courant Coe cient

At this stage it is necessary to introduce the Courant or CFL coe cient, a ratio that will prove invaluable when seeking accuracy from the solvers. The CFL condition is a necessary condition that must be satis ed by any nite volume or nite di erence method in order to provide stability and hence convergence to the solution of a di erential equation as the grid is re ned. Leveque summarised the condition as

CFL Condition

that no wave present in the solution of all Riemann problems travels more than a distance x in time t. For the time-dependent, one dimensional Euler equations, we can estimate $S^n_{\max}$ as

$$S^n_{\max} = \max_i \left(S^L_{i+\frac{1}{2}} \; ; \; S^R_{i+\frac{1}{2}} \right) ; \tag{4.3}$$

for $i = 0;:::;M$, where $S^L_{i+\frac{1}{2}}$, $S^R_{i+\frac{1}{2}}$ are the wave speeds of the left and right non-linear waves present in the solution of the Riemann problem $R\left(\mathbf{U}^n_i; \mathbf{U}^n_{i+1}\right)$. The Riemann problem generates three waves; non-linear waves, which can be shocks or rarefactions and are the fastest waves. For rarefaction waves we select the speed of the head and for shock waves we select the shock speed. It is important to note that when sampling the wave speeds we must include the boundaries, as these may generate large wave speeds. By using (4.3) to find $S^n_{\max}$ and thus t of (4.1) we have a simple and reliable procedure [20].

4.3 Boundary Conditions

Boundary conditions are needed at the boundaries $x = 0$ and $x = L$ for a domain $[0; L]$ discretised into M computing cells of length x. In addition, the boundary conditions provide the numerical fluxes $\mathbf{F}_{\frac{1}{2}}$, and $\mathbf{F}_{M+\frac{1}{2}}$. We require these in order to apply the conservative formula (3.5) to update the extreme cells I_1 and I_M to the next time level $n + 1$, and they may result directly in $\mathbf{F}_{\frac{1}{2}}$ and $\mathbf{F}_{M+\frac{1}{2}}$. We can also force fictious data values in the fictious cells I_0 and I_{M+1}, adjacent to I_1 and I_M. By doing this, boundary Riemann problems are solved and the corresponding Godunov fluxes are computed [20].

We consider two types of boundary conditions in this study, *reflective* and *transparent* conditions.

4.3.1 Reflective boundaries

Reflective boundaries refer physically to walls at either side of the domain. We can think of it as a boundary $x = L$ then the physical situation is modelled creating a fictitious state $W_{(M+1)^n}$ to the right of the boundary and defining the boundary Riemann problem as $R(W^{(}_M n); W_{(M+1)^n})$. This fictitious state is defined from the state W^n_M inside the computational domain, in other words

$$\rho^n_{M+1} = \rho^n_M ; \; u^n_{M+1} = -u^n_M ; \; p^n_{M+1} = p^n_M : \tag{4.4}$$

The exact solution of this depends on the value of u^n_M, if it is greater than zero the solution consists of two shock waves. If it is less than or equal to zero there are two rarefaction waves. For both

scenarios *u*

5 Approximate Riemann Solvers

These approximate Riemann solvers are introduced in chronological order.

5.1 Roe (1981)

The Roe solver, devised by Roe [12], is an approximate Riemann solver based around the Godunov scheme and works by looking for an estimate for the intercell numerical ux or Godunov ux $F_{i+\frac{1}{2}}$ at the interface between two computational cells U_i and $U_{i+\frac{1}{2}}$ on a discretised space-time computational domain.

5.1.1 The Original Roe Method

To determine the Godunov method we need to nd the average eigenvalues $\tilde{}_i$, the corresponding averaged right eigenvectors $\tilde{K}^{(i)}$ and averaged wave strengths $\tilde{}_i$. In the 1981 paper [12] an averaged Jacobian matrix $\tilde{A}$, the Roe matrix, is found and from which $\tilde{}_i$, $\tilde{K}^{(i)}$ and $\tilde{}_i$ follow. In the matrix $\tilde{A}$ the properties (A)-(C) are enforced.

Property (A): Hyperbolicity of the system. $\tilde{A}$ is required to have real eigenvalues $\tilde{}_i = \tilde{}_i(U_L; U_R)$, which we choose to order as

$$\tilde{}_1 \leq \tilde{}_2 \leq \cdots \leq \tilde{}_m \tag{5.1}$$

and a complete set of linearly independent right eigenvectors

$$\tilde{K}^{(1)}, \tilde{K}^{(2)}, \ldots, \tilde{K}^{(m)}. \tag{5.2}$$

Property (B): Consistency with the exact Jacobian

$$\tilde{A}(U; U) = A(U). \tag{5.3}$$

Property (C): Conservation across discontinuities

$$F(U_R) - F(U_L) = \tilde{A}(U_R - U_L) \tag{5.4}$$

Property (C) is the crucial property, as it narrows choices for $\tilde{A}$. Roe showed that the existence of a matrix $\tilde{A}$ satisfying property (C) is assured by the mean value theorem [12]. To nd the vector

A, Roe introduced the idea of a *parameter vector* Q, such that both the vector of conserved variables U and the ux vector F(U) could be expressed in terms of Q. That is

$$U = U(Q); \quad F = F(Q): \tag{5.5}$$

This is followed by two important steps. First the changes

$$U = U_R \quad U_L; \quad F = F(U_R) \quad F(U_L) \tag{5.6}$$

can be expressed in terms of the change $Q = Q_R \quad Q_L$. And secondly, averages are obtained in terms of *simple arithmetic means* of Q. We now illustrate the technique as applied to the Euler equations in one dimension.

The Euler equations Here we present the Roe Riemann solver as applied to the Riemann problem for the *x*-split one dimensional time dependent Euler equations for ideal gases.

The exact *x*-direction Jacobian matrix A(U) is

$$A = \begin{matrix} 2 \\ 6 \\ 6 \\ 6 \end{matrix}$$

[8.]TJ/FH.9626 Tf 8.383 1.49[1.30500

Roe then chooses the *parameter vector*

$$Q \equiv \begin{bmatrix} q_1 \\ q_2 \\ q_3 \end{bmatrix} \equiv \begin{bmatrix} \sqrt{\rho} \\ \sqrt{\rho}\, u \\ H \end{bmatrix}; \tag{5.13}$$

in which every component u_i of U and every component f_i of $F(U)$ in (??)-(??) is a quadratic in the components q_i of Q. In other words, $u_1 = q_1^2$ and $f_1 = q_1 q_2$, and so on. In fact, the property is valid for the components of the G and H fluxes for the full three-dimensional Euler equations.

The jumps ΔU and ΔF can be expressed in terms of the jump ΔQ via two matrices B and C. Roe [12] gives the following expressions

$$B = \begin{bmatrix} 2\bar{q}_1 & 0 & 0 \\ \bar{q}_2 & \bar{q}_1 & 0 \\ \bar{q}_3 & \frac{1}{2}\bar{q}_2 & \bar{q}_1 \end{bmatrix} \tag{5.14}$$

and

$$C = \begin{bmatrix} \bar{q}_2 & \bar{q}_1 & 0 \\ \frac{1}{2}\bar{q}_3 & \frac{1}{2}\bar{q}_2 & \frac{\bar{q}_1}{2} \\ 0 & \bar{q}_3 & \bar{q}_2 \end{bmatrix}. \tag{5.15}$$

The Roe matrix is then given by

$$\bar{A} = BC^{-1}. \tag{5.16}$$

The eigenvalues of $\bar{A}$ are

$$\tilde{\lambda}_1 = \bar{u} - \bar{a}, \quad \tilde{\lambda}_2 = \tilde{\lambda}_3 = \tilde{\lambda}_4 = \bar{u}, \quad \tilde{\lambda}_5 = \bar{u} + \bar{a} \tag{5.17}$$

and the corresponding right eigenvectors are

$$\bar{K}^{(1)} = \begin{bmatrix} 1 \\ \bar{u} - \bar{a} \\ \bar{H} - \bar{u}\bar{a} \end{bmatrix}, \quad \bar{K}^{(2)} = \begin{bmatrix} 1 \\ \bar{u} \\ \frac{1}{2}\bar{u}^2 \end{bmatrix}, \quad \bar{K}^{(3)} = \begin{bmatrix} 1 \\ \bar{u} + \bar{a} \\ \bar{H} + \bar{u}\bar{a} \end{bmatrix}. \tag{5.18}$$

The symbol $\bar{r}$ in (5.17), (5.18)denotes a Roe average for a variable r. The relevant averages are given as follows

$$\begin{aligned} \bar{u} &= \frac{\sqrt{\rho_L}u_L + \sqrt{\rho_R}u_R}{\sqrt{\rho_L} + \sqrt{\rho_R}}, \\ \bar{H} &= \frac{\sqrt{\rho_L}H_L + \sqrt{\rho_R}H_R}{\sqrt{\rho_L} + \sqrt{\rho_R}}, \\ \bar{a} &= (\gamma - 1)\left[\bar{H} - \tfrac{1}{2}\bar{u}^2\right]. \end{aligned} \tag{5.19}$$

To determine the Roe numerical flux $F_{i+\frac{1}{2}}$ it is neccessary to have the wave strengths $\tilde{\alpha}_i$. These can be obtained by projecting the jump ΔU onto the right, averaged eigenvectors (5.18), that is

$$\Delta U = \sum_{i=1}^{3} \tilde{\alpha}_i \bar{K}^{(i)}$$

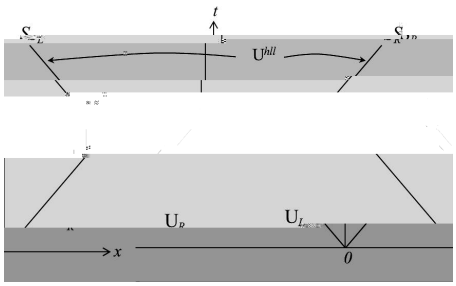

Figure 5.1: Approximate HLL Riemann solver. Solution in the *Star Region* consists of a single state $\mathbf{U}^{hll}$ separated from data states by two waves of speeds S_L and S_R

For a review of the Godunov method, we can refer back to Section 3. We recall the Godunov intercell numerical ux

$$F_{i+\frac{1}{2}} = F(U_{i+\frac{1}{2}}(0)); \tag{5.24}$$

where $U_{i+\frac{1}{2}}(0)$ is the exact similarity solution $U_{i+\frac{1}{2}}(x=t)$ of the Rieman problem

$$\begin{aligned} &U_t + F(U)_x = 0 \\ &U(x;0) = \begin{cases} U_L \ if \ x < 0; \\ U_R \ if \ x > 0; \end{cases} \end{aligned} \tag{5.25}$$

evaluated at $x=t = 0$. The solver devised by Harten, Lax and van Leer [7] sets out to nd direct approximations to the ux function $F_{i+\frac{1}{2}}$. They put forward the following approximate Riemann solver

$$U(x;t) = \begin{cases} U_L \ if \ \frac{x}{t} \leq S_L; \\ U^{hll} \ if \ S_L \leq \frac{x}{t} \leq S_R; \\ U_R \ if \ \frac{x}{t} > S_R; \end{cases} \tag{5.26}$$

where U^{hll} is the constant state vector given by

$$U^{hll} = \frac{S_R U_R - S_L U_L + F_L - F_R}{S_R - S_L}; \tag{5.27}$$

and the speeds S_L and S_R are known values. If we consider imaginary graph 5.1, which shows the structure of this approximate solution, we can see that it consists of three constant states separated by two waves. The *Star Region* consists of a *single* constant state; all intermediate states separated by intermediate waves are *lumped* into the single state U^{hll}. It is important to make note that we do not take $F^{hll} = F(U^{hll})$. The area of interest is the subsonic case $S_L \leq 0 \leq S_R$. Substituting U^{hll} in (5.27) yields

$$F^{hll} = F_L + S_L(U^{hll} - U_L); \tag{5.28}$$

or

$$\mathbf{F}^{hll} = \mathbf{F}_R + S_R(\mathbf{U}^{hll} - \mathbf{U}_R). \tag{5.29}$$

Use of (5.27) on (5.28) and (5.29) results in the HLL flux

$$\mathbf{F}^{hll} = \frac{S_R\mathbf{F}_L - S_L\mathbf{F}_R + S_LS_R(\mathbf{U}_R - \mathbf{U}_L)}{S_R - S_L}. \tag{5.30}$$

Which can be used to produce the corresponding intercell flux for the approximate Gudonov method

$$F^{hll}_{i+1} = \begin{cases} F_L \ if \ 0 \leq S_L; \\ \frac{S_R\mathbf{F}_L - S_L\mathbf{F}_R + S_LS_R(\mathbf{U}_R - \mathbf{U}_L)}{S_R - S_L}; \ if \ S_L \leq 0 \leq S_R; \\ F_R \ if \ 0 \geq S_R. \end{cases} \tag{5.31}$$

We will discuss the calculation of S_L and S_R after the discussion on the HLLC solver, in Section 5.2.2, but given those speeds we can use (5.31) in the conservative formula (5.23) to get an approximate Godunov method. In their paper, Harten, Lax and van Leer [7] showed that this Godunov scheme converges to the weak solution of conservation laws and proved that the converged solution is also the physical, entropy satisfying, solution of the conservation laws [20]. The requirements for this include that an approximate solution $\mathbf{U}(x,t)$ is consistent with the integral form of the

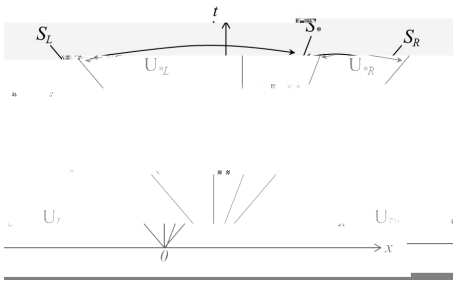

Figure 5.2: Approximate HLLC Riemann solver. Solution in the *Star Region* consists of two constant states separated by a middle wave speed of S_*.

sponding to the multiple eigenvalue $_2 = {}_3 = {}_4 = u$. The integral form of the conversation laws does not change from (5.33) even with variations of the integrand across S_*. With this addition, the consistency condition 5.32 becomes e ectively the condition (5.33), and thus by splitting the left-hand side of (5.33) into two terms we obtain

$$\begin{aligned}\frac{1}{T(S_R - S_L)} \int_{TS_L}^{TS_R} \mathbf{U}(x;T)dx = &\frac{1}{T(S_R - S_L)} \int_{TS_L}^{TS_*} \mathbf{U}(x;T)dx \\ &+ \frac{1}{T(S_R - S_L)} \int_{TS_*}^{TS_R} \mathbf{U}(x;T)dx\end{aligned} \tag{5.34}$$

And the integral averages are de ned as

$$\begin{aligned}\mathbf{U}_L &= \frac{1}{T(S_R - S_L)} \int_{TS_L}^{TS_*} \mathbf{U}(x;T)dx; \\ \mathbf{U}_R &= \frac{1}{T(S_R - S_L)} \int_{TS_*}^{TS_R} \mathbf{U}(x;T)dx:\end{aligned} \tag{5.35}$$

Substituting (5.35) into (5.34) and using (5.33), The Consistency Cona9738 Tf 285.659 738 T19738 Tf 211.J 0 -2.9

5.2.2 Wave-speed estimates

To allow for the calculation of the uxes in both the HLL and HLLC schemes it is necessary to have algorithms for computing wave speeds. We just require speeds S_L and S_R for the HLL scheme, but require the additional middle wave speed S for the HLLC scheme. We will look at two ways of estimating S_L, S_R and S : direct estimates and pressure-velocity estimates.

Direct wave speed estimates The direct wave speed estimates are the most simple methods providing minimum and maximum signal velocities. The most simple of these is provided by Davis [2]

$$S_L = u_L \quad a_L; \; S_R = u_R + a_R \tag{5.47}$$

and

$$S_L = \min fu_L \quad a_L; u_R \quad a_R g; \; S_R = \max fu_R + a_R; u_R + a_R g: \tag{5.48}$$

Because of the simplicity of these estimates, it is necessary to look at more complex estimates. We can also make use of the Roe [11] average eigenvalues, that we use in the Roe Riemann scheme, for the left and right non-linear waves

$$S_L = \breve{u} \quad \breve{a}; \; S_R = \breve{u} + \breve{a}; \tag{5.49}$$

where $\breve{u}$ and $\breve{a}$ are the Roe-average particle and sound speeds respectively, given as

$$\breve{u} = \frac{\sqrt{\rho_L}u_L + \sqrt{\rho_R}u_R}{\sqrt{\rho_L} + \sqrt{\rho_R}}; \; \breve{a} = \left(\quad 1\right) \breve{H} \quad \frac{1}{2}\breve{u}^2 \quad ^{\frac{1}{2}}; \tag{5.50}$$

with the enthalpy $H = (E + p)=$ approximated as

$$\breve{H} = \frac{\sqrt{\rho_L}H_L + \sqrt{\rho_R}H_R}{\sqrt{\rho_L} + \sqrt{\rho_R}}: \tag{5.51}$$

More information about the Roe solver and scheme are given in the previous chapter. The Rusanov ux can be obtained by, is taking a positive speed S^+, setting $S_L = \quad S^+$ and $S_R = S^+$ in the HLL ux (refeq:10.21), as observed by Davis [14]

F

which is bounded by [20]

$$S^+ = \max\{|u_L| + a_L, |u_R| + a_R\}. \tag{5.54}$$

Both are considered and investigated in Section 7. Finally we consider the Einfeldt eigenvalues [4], which are motivated by the Roe values

$$S_L = \bar{u} - \bar{d}, \quad S_R = \bar{u} + \bar{d}, \tag{5.55}$$

where

$$\bar{d}^2 = \frac{\sqrt{\rho_L}a_L^2 + \sqrt{\rho_R}a_R^2}{\sqrt{\rho_L} + \sqrt{\rho_R}} + \eta_2(u_R - u_L)^2 \tag{5.56}$$

and

$$\eta_2 = \frac{1}{2}\frac{\sqrt{\rho_L}\sqrt{\rho_R}}{(\sqrt{\rho_L} + \sqrt{\rho_R})^2}. \tag{5.57}$$

Comparisons of the results given by these various wave speeds can be seen in (the following section).

Pressure-velocity based wave speed estimates Finding wave speed estimates by estimating the pressure p

The approximations given in 5.60 and 5.61 can be used in (5.58) - (5.59) to obtain wave speed estimates for the HLL and HLLC schemes. There are other ways to approximate p and u, such as the Two-Rarefaction Riemann solver, but due to time restraints these were not investigated (see Toro sect 9.4.1).

5.3 Osher-Solomon (1982)

The final scheme being considered in this study is the Osher-Solomon scheme, devised as an upwind finite difference approximation to systems of nonlinear hyperbolic conservation laws [9]. It is an attractive scheme due to the smoothness of the numerical flux; proving to be entropy satisfying and in practical computations it is seen to handle the sonic flow well [20]. This chapter will look at how to apply the Osher-Solomon method to nonlinear hyperbolic conservation laws, looking specifically at the Euler equations, and will describe the two-different methods of ordering the flux for computation.

5.3.1 Osher-Solomon for the Euler equations

In this section we take the time-dependent Euler equations and develop the Osher-Solomon scheme for them, with both P and O orderings. We consider first the one-dimensional case

$$U_t + F(U)_x = 0 \tag{5.62}$$

$$U = \begin{bmatrix} \rho \\ \rho u \\ E \end{bmatrix}; \quad F(U) = \begin{bmatrix} \rho u \\ \rho u^2 + p \\ u(E + p) \end{bmatrix}; \tag{5.63}$$

Where we have considered the details of these equations in Chapter 2. The explicit conservative formula requires us to have an expression for the intercell flux $F_{i+\frac{1}{2}}$

i8y

F

$$U_i^{n+1} = U_i^n +$$

and right eigenvectors

$$K^{(1)} = \begin{bmatrix} 1 & & \\ u & a & \\ H & ua & \end{bmatrix}; \quad K^{(2)} = \begin{bmatrix} 1 & & \\ u & & \\ \frac{1}{2}u^2 & & \end{bmatrix}; \quad K^{(3)} = \begin{bmatrix} 1 & & \\ u+a & & \\ H+ua & & \end{bmatrix}: \tag{5.66}$$

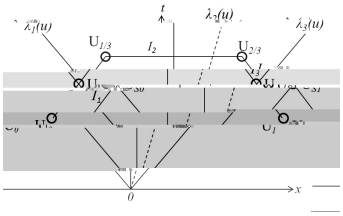

Figure 5.3: Possible con guration of integration paths $I_k(\mathbf{U})$, intersection points $\mathbf{U}_{\frac{1}{3}}$, $\mathbf{U}_{\frac{2}{3}}$ and sonic points $\mathbf{U}_{S0}$, $\mathbf{U}_{S1}$ in physical space $x-t$ for a 3 by 3 system

5.3354n(system)]T -1.107 Td 4ws701 Tf

the intersection points $U_{\frac{1}{3}}$ and $U_{\frac{2}{3}}$ are approximations [20]. The underlying assumption here though is that both nonlinear waves are rarefaction which corresponds to the Two-Rarefaction approximation TRRS (see [20] section 9.4.1). By using (5.67) across the left wave we get

$$u + \frac{2a_{\frac{1}{3}}}{1} = u_0 + \frac{2a_0}{1} \tag{5.69}$$

and similarly using (5.68) across the right wave

$$u \quad \frac{2a_{\frac{2}{3}}}{1} = u_1 \quad \frac{2a_1}{1} \tag{5.70}$$

where u is the common particle velocity for $U_{\frac{1}{3}}$ and $U_{\frac{2}{3}}$. We also know that the pressure p is also common

$$u_{\frac{1}{3}} = u_{\frac{2}{3}} = u = \text{constant}; \; p_{\frac{1}{3}} = p_{\frac{2}{3}} = p = \text{constant}. \tag{5.71}$$

Applying the isentropic law, that entropy is constant, to the left and right waves gives

$$a_{\frac{1}{3}} = a_0(p = p_0)^z; \; a_{\frac{2}{3}} = a_1(p = p_1)^z; \tag{5.72}$$

with

$$z = \frac{1}{2}: \tag{5.73}$$

Using (5.69) and (5.72) we get

$$u = u_0 \quad \frac{2a_0}{1} \quad \left(\frac{p}{p_0}\right)^z \quad 1 \; : \tag{5.74}$$

And by using (5.70) and (5.72)

$$u = u_1 + \frac{2a_1}{1} \quad \left(\frac{p}{p_1}\right)^z \quad 1 \; : \tag{5.75}$$

Solving for p and u we obtain

$$p = \left(\frac{a_0 + a_1 \quad (u_1 \quad u_0)(\quad 1)=2}{a_0=p_0^z + a_1=p_1^z}\right)^{\frac{1}{z}}; \tag{5.76}$$

$$u = \frac{Hu_0=a_0 + u_1=a_1 + 2(H \quad 1)(\quad 1)}{H=a_0 + 1=a_1}; \tag{5.77}$$

with

$$H = (p_0=p_1)^z:$$

The values for the densities $_{\frac{1}{3}}$ and $_{\frac{2}{3}}$ equate to

$$_{\frac{1}{3}} = \; _0 \left(\frac{p}{p_0}\right)^{\frac{1}{}}; \quad _{\frac{2}{3}} = \; _1 \left(\frac{p}{p_1}\right)^{\frac{1}{}}: \tag{5.78}$$

And thus the complete solution for $U_{\frac{1}{3}}$, $U_{\frac{2}{3}}$ is given by (5.76) - (5.78). In order to compute the sonic points U_{S0} and U_{S1} we first enforce the sonic conditions $_1 = u \quad a = 0$ and $_3 = u + a = 0$

and then by applying the Generalised Riemann Invariants [20]. The solution for the left sonic point becomes

$$\left.\begin{aligned} u_{S0} &= \tfrac{1}{\gamma+1}u_0 + \tfrac{2a_0}{\gamma+1};\ a_{S0} = u_{S0};\\ \rho_{S0} &= \rho_0\left(\tfrac{a_{S0}}{a_0}\right)^{\frac{2}{\gamma-1}};\ p_{S0} = p_0\left(\tfrac{\rho_{S0}}{\rho_0}\right)^{\gamma}; \end{aligned}\right\} \tag{5.79}$$

Similarly, for the right sonic point

$$\left.\begin{aligned} u_{S1} &= \tfrac{1}{\gamma+1}u_1 - \tfrac{2a_1}{\gamma+1};\ a_{S1} = -u_{S1};\\ \rho_{S1} &= \rho_1\left(\tfrac{a_{S1}}{a_1}\right)^{\frac{2}{\gamma-1}};\ p_{S1} = p_1\left(\tfrac{\rho_{S1}}{\rho_1}\right)^{\gamma}; \end{aligned}\right\} \tag{5.80}$$

Integration along partial paths. For the Osher-Solomon intercell flux we use

$$\mathbf{F}_{i+\frac{1}{2}} = \mathbf{F}_0 + \int_{\mathbf{U}_0}^{\mathbf{U}_1} \mathbf{A}(\mathbf{U})d\mathbf{U};$$

Next, we find the sonic points U_{S0} and U_{S1} by first connecting U_0 and $U_{\frac{1}{3}}$ via the *right* Riemann Invariant

$$u_{S0} = \frac{2a_{S0}}{1} + u_{\frac{1}{3}}$$

	$u_0 + a_0 > 0$ $u_1 + a_1 > 0$	$u_0 + a_0 > 0$ $u_1 \quad a_1 \ 6 \ 0$	$u_0 + a_0 \ 6 \ 0$ $u_1 \quad a_1 > 0$	$u_0 + a_0 \ 6 \ 0$ $u_1 + a_1 \ 6 \ 0$
$u \quad + a_{\frac{1}{3}} \ 6 \ 0$	$F_0 \quad F_{S0} + F_{S1}$	$F_0 \quad F_{S0} + F_1$	F_{S1}	F_1
$u \quad + a_{\frac{1}{3}} > 0; \ u \quad 6 \ 0$	$F_0 \quad F_{\frac{1}{3}} + F_{S1}$	$F_0 \quad F_{\frac{1}{3}} + F_1$	$F_{S0} \quad F_{\frac{1}{3}} + F_{S1}$	$F_{S0} \quad F_{\frac{1}{3}} + F_1$
u				

numerical flux at the interface of two states U_L, U_R is

$$F^{LF}_{i+\frac{1}{2}} = F^{LF}_{i+\frac{1}{2}}(U_L; U_R) = \frac{1}{2}[F(U_L) + F(U_R)] + \frac{1}{2}\frac{x}{t}[U_L \quad U_R]: \tag{6.2}$$

Minmod

$$\phi_{sb}(r) = \begin{cases} 0; & r \leq 0; \\ 2r; & 0 \leq r \leq \frac{1}{2}; \\ 1; & \frac{1}{2} \leq r \leq 1; \\ \min\{2; \ \psi_g + (1 - \psi_g)rg; & r > 1. \end{cases} \tag{6.10}$$

Superbee

$$\phi_{vl}(r) = \begin{cases} 0; & r \leq 0; \\ \frac{2r}{1+r}; & 0 \leq r \leq 1; \\ \psi_g + \frac{2(1-\psi_g)r}{1+r}; & r > 1. \end{cases} \tag{6.11}$$

van Leer

$$\phi_{vl}(r) = \begin{cases} 0; & r \leq 0; \\ r; & 0 \leq r \leq 1; \\ 1; & r > 1. \end{cases} \tag{6.12}$$

De ning the total energy q E and setting

$$r^L_{i+\frac{1}{2}} = \frac{q_{i-\frac{1}{2}}}{q_{i+\frac{1}{2}}}; \ r^R_{i+\frac{1}{2}} = \frac{q_{i+\frac{3}{2}}}{q_{i+\frac{1}{2}}}. \tag{6.13}$$

(6d503l)]TJ/k626 Tf96.473 32.47 d504 6d503l

7 Comparison of Schemes

All schemes required tweaking of CFL for each test case. In all tests, data consists of two constant states $\mathbf{W}_L = [\ _L; u_L; p_L]^T$ and $\mathbf{W}_R = [\ _R; u_R; p_R]^T$ with a discontinuity in the middle of the states at position $x = x_0$. Numerical solutions are presented with exact solutions and are found

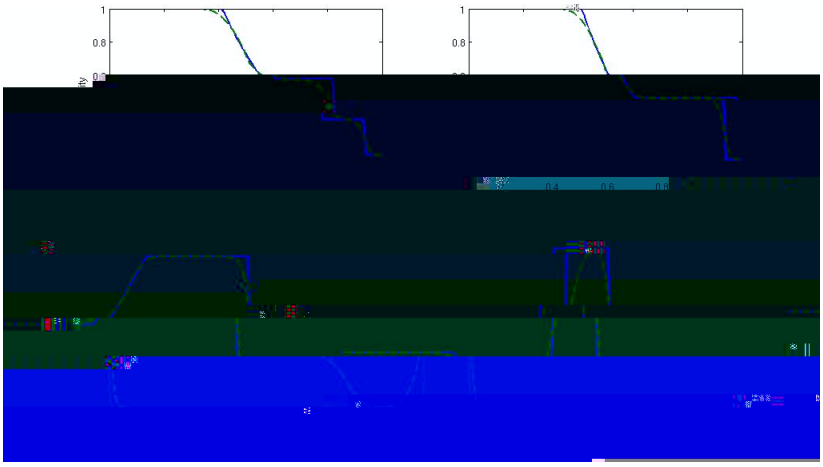

Figure 7.1: Roe Riemann solver applied to Test 1 of Table 7.1. Numerical (dash) and exact (line) solutions compared at time 0.2

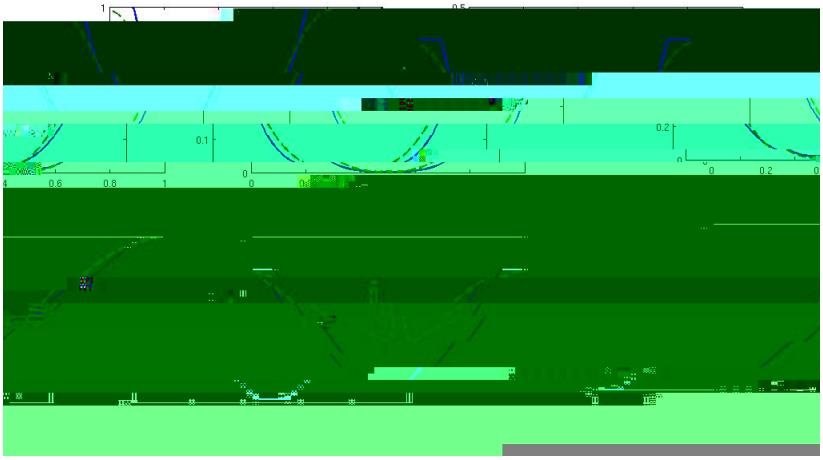

Figure 7.2: Roe Riemann solver applied to test 2 of Table 7.1. Numerical (dash) and exact (line) solutions compared at time 0.15

Test 2 consists of two symmetric rarefaction waves and a trivial contact wave, with the star

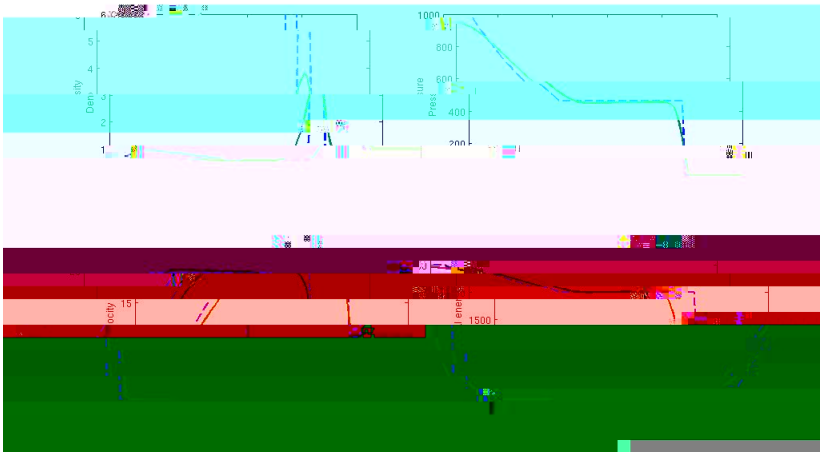

Figure 7.3: Roe Riemann solver applied to test 3 of Table 7.1. Numerical (dash) and exact (line) solutions compared at time 0.012

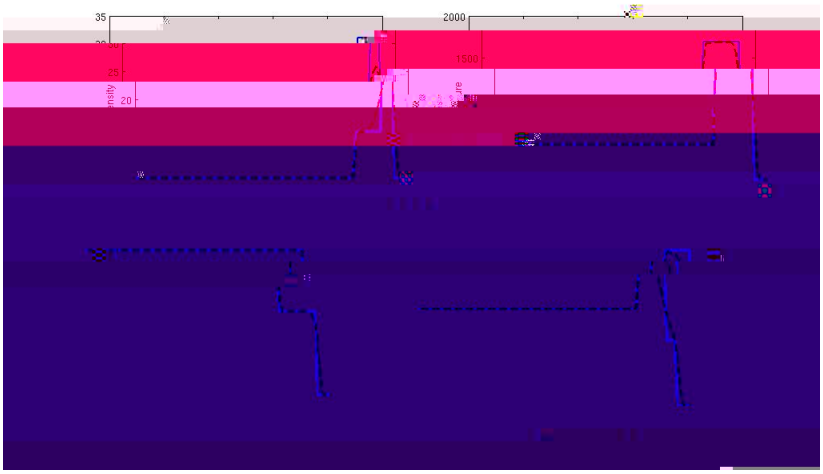

Figure 7.4: Roe Riemann solver applied to test 4 of Table 7.1. Numerical (dash) and exact (line) solutions compared at time 0.012

wave speed estimates were, therefore it was discarded and the results are not shown here. If we consider Figures 7.6 to 7.11 we can see that there is little deviation in precision, but considering the Figures 7.8 and 7.9 we can see that the Roe eigenvalue estimates (5.49) provide disappointing results, as do the Davis estimates (5.53) and these were also not considered. The simpler estimates (5.47) and (5.48), shown in Figures 7.6 and 7.7 respectively, gave fairly accurate results for their computational simplicity, but ultimately Einfeldt's estimate (5.55) shown in Figure 7.10 was more accurate, and simple enough, so this was chosen as the wave speed estimate for all following tests using the HLL scheme. The final wave speed estimate, the PVRS estimate, was shown in Figure 7.11 to be as precise as Einfeldt, thus sufficient for the HLLC scheme that requires the pressure value for the star region.

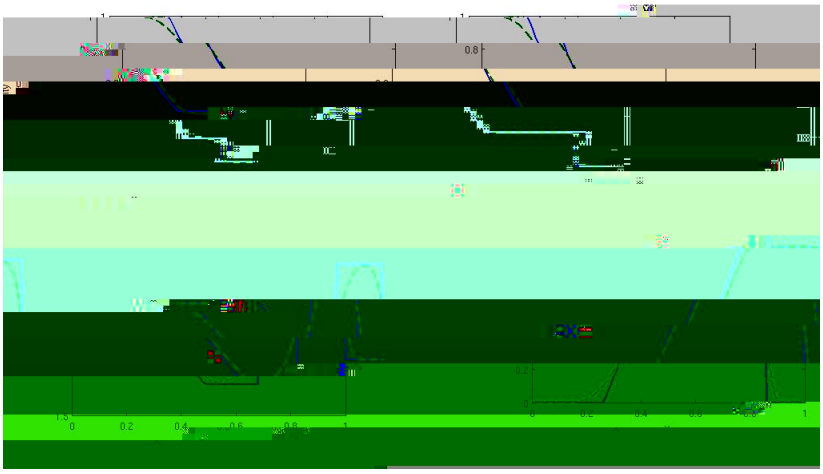

Figure 7.6: HLL Riemann solver applied to Sod's shock tube, using wave speed estimate (5.48). Numerical (dash) and exact (line) solutions compared at time 0.20

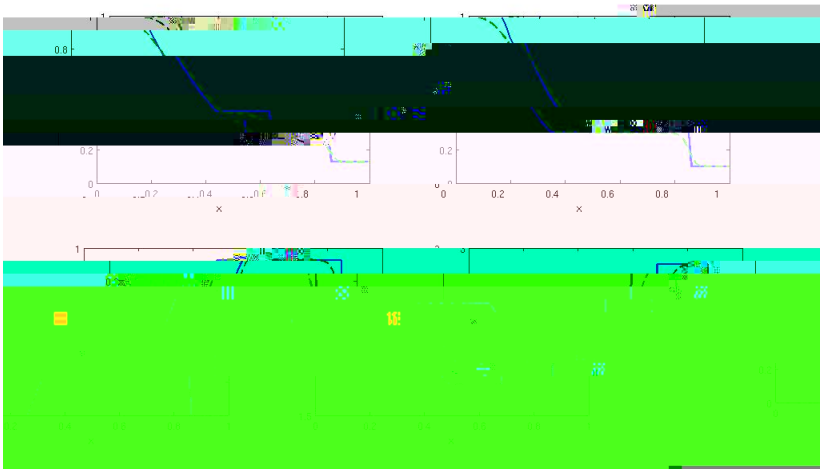

Figure 7.7: HLL Riemann solver applied to Sod's shock tube, using wave speed estimate (5.49). Numerical (dash) and exact (line) solutions compared at time 0.20

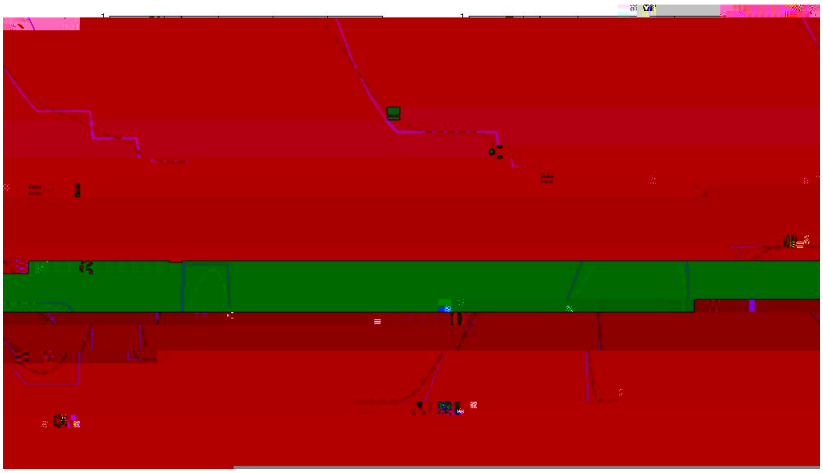

Figure 7.8: HLL Riemann solver applied to Sod's shock tube, using wave speed estimate (5.53). Numerical (dash) and exact (line) solutions compared at time 0.20

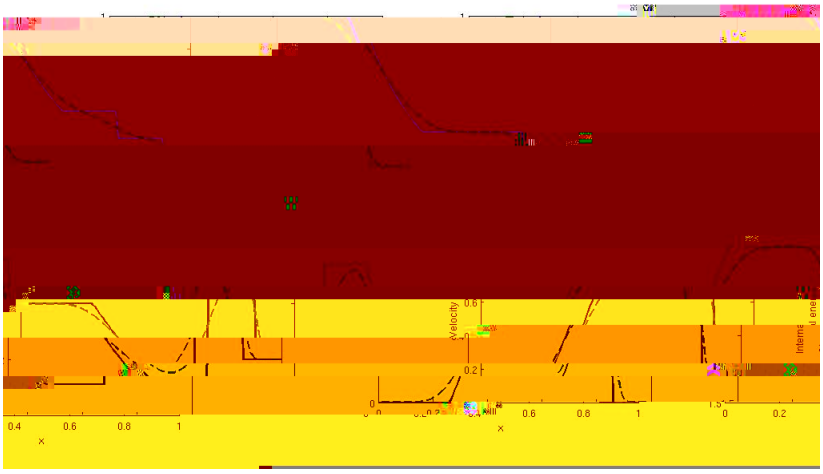

Figure 7.9: HLL Riemann solver applied to Sod's shock tube, using wave speed estimate (5.54). Numerical (dash) and exact (line) solutions compared at time 0.20

Figure 7.10: HLL Riemann solver applied to Sod's shock tube, using wave speed estimate (5.55). Numerical (dash) and exact (line) solutions compared at time 0.20

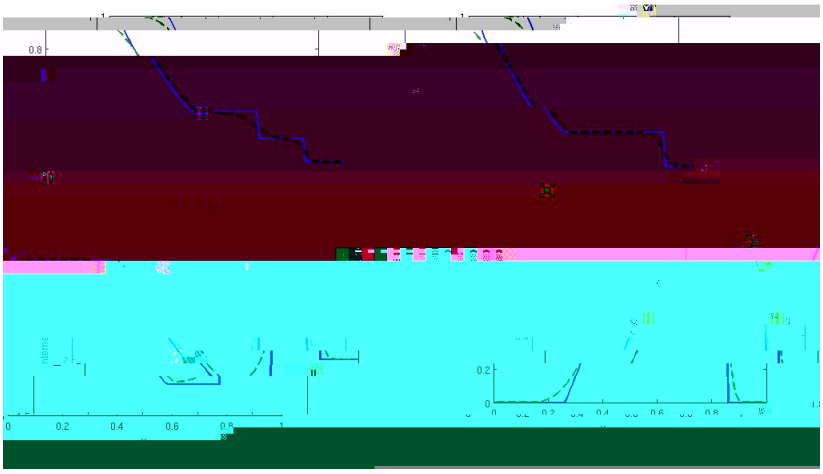

Figure 7.11: HLL Riemann solver applied to Sod's shock tube, using wave speed estimate (5.58). Numerical (dash) and exact (line) solutions compared at time 0.20

7.2.2 Test problems

To test the HLL scheme, modi ed versions of the problems described in Section 2.3, outlined in Table 7.2. Numerical solutions are computed with $M = 100$ cells. Boundary conditions are transparent with the exception of the blast wave tests, which use re ective boundaries, due to walls being present at either side of the domain.

Test	$_L$	u_L	p_L	$_R$	u_R	p_R
1	1.0	0.75	1.0	0.125	0.0	0.1
2	1.0	-2.0	0.4	1.0	2.0	0.4
3	1.0	0.0	1000.0	1.0	0.0	0.01
4	5.99924	19.5975	460.894	5.99242	-6.19633	46.0950
5	1.0	-19.5975	1000.0	1.0	-19.5975	0.01
6	1.4	0.0	1.0	1.0	0.0	1.0
7	1.4	0.1	1.0	1.0	0.1	1.0

Table 7.2: Data for test problems for the HLL and HLLC schemes

These tests were rst presented by Toro [20] in order to assess speci c parts of the schemes. All were conducted as ideal gases with = 1:4, with two constant states separated by a discontinuity at $x = x_0$. The exact and numerical solutions are found in the domain 0 x 1, and the numerical solutions were computed with $M = 100$ cells and the CFL was kept at 0.5. Boundary

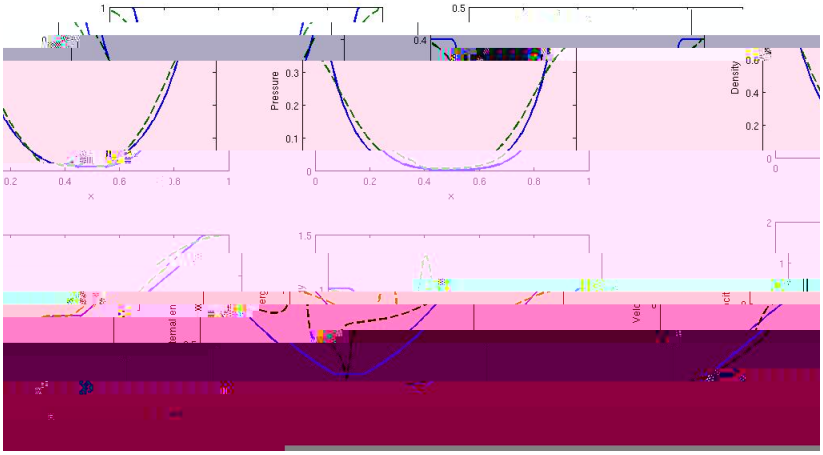

Figure 7.14: HLLC Riemann solver applied to Test 2 of Table 7.2. Numerical (dash) and exact (line) solutions compared at time 0.15 and $x_0 = 0.5$

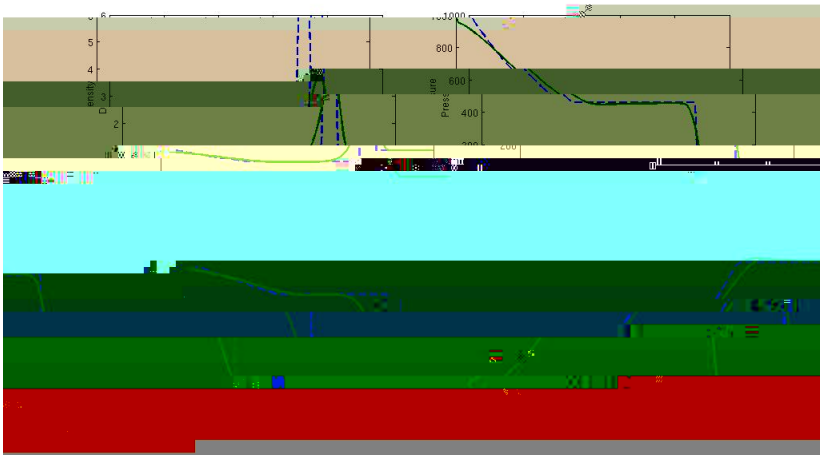

Figure 7.15: HLL Riemann solver applied to the left-hand side of the Blast Wave problem, Test 3 of 7.2. Numerical (dash) and exact (line) solutions compared at time 0.012 and $x_0 = 0.5$

Test 2's solution concerns itself with two symmetric rarefaction waves and a trivial contact wave. Between the linear waves, the star region is close to vacuum, making the problem a good test for assessing the performance of the approximate Riemann solvers for low-density flows. The first point to note is that the HLL solver was not robust enough to produce satisfactory results for this test, and has therefore not been plotted. The HLLC solver, shown in Figure 7.27, produced fairly accurate results, but broke down when dealing with the internal energy of the system.

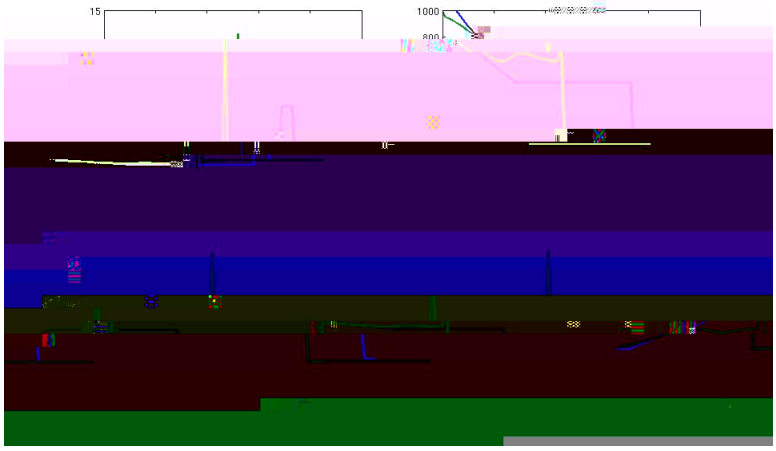

Figure 7.16: HLLC Riemann solver applied to Test 3 of Table 7.2. Numerical (dash) and exact (line) solutions compared at time 0.012 and $x_0 = 0.5$

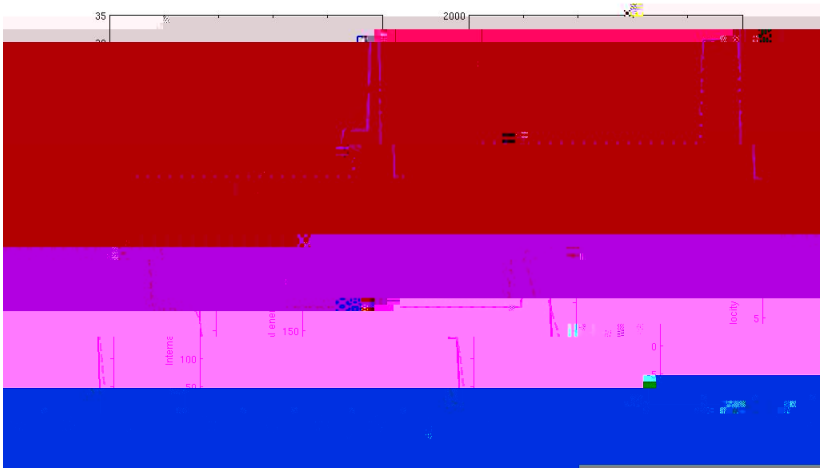

Figure 7.17: HLL Riemann solver applied to Test 4 of Table 7.2. Numerical (dash) and exact (line) solutions compared at time 0.012 and $x_0 = 0.4$

Accuracy and robustness is tested using test 3, the solution of which consists of a strong shock wave, a contact surface and a left rarefaction wave. The strong shock wave is of Mach number 198, where the Mach number is the speed of an object moving through a uid divided by the speed of sound in that uid for its particular physical conditions, including those of temperature and pressure, it is a dimensionless quantity. We can see in Figure 7.29 that the HLL scheme is fairly robust, but struggles somewhat to represent accurate density, this result is unexpected as we would expect it to perform better than the HLL solver.

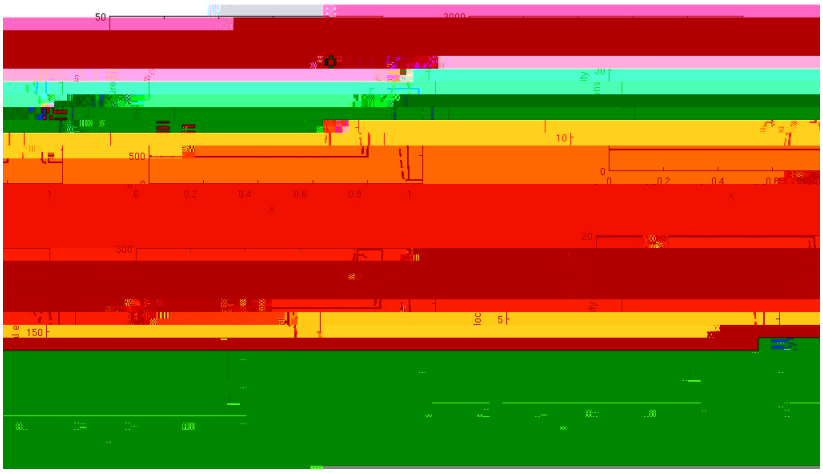

Figure 7.18:

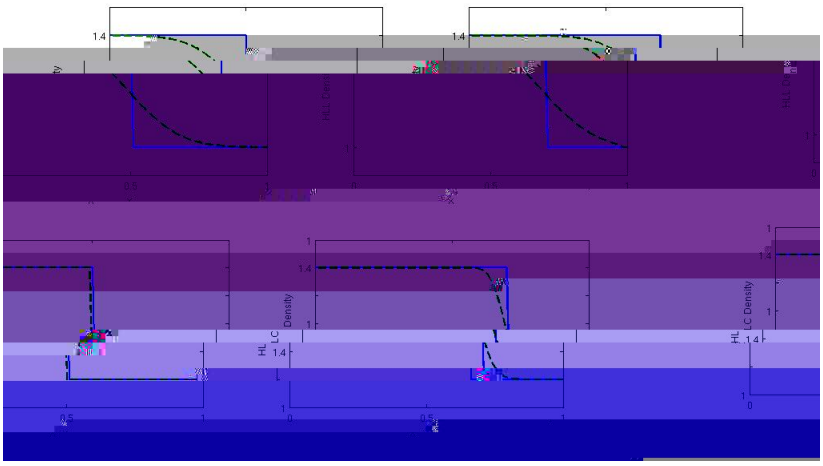

Figure 7.20: Density pro les for the HLL and HLLC Riemann solvers applied to tests 6 and 7, with wave speed estimate Einfeldt (5.55). Numerical (dash) and exact (line) solutions compared at time 0.20

The solution of test 5 consists of a right-travelling shock wave, a left rarefaction wave and a stationary contact discontinuity. Looking at Figure 7.19, we can see that the HLL Riemann solver di uses the contact wave to less precise levels. This should highlight the advantage of HLLC over HLL in the resolution of slowly-moving contact discontinuities, however we were unable to produce a satisfactory result with the HLLC scheme. This observation is however emphasised by Tests 6 and 7. Tests 6 and 7 shown in Figure 7.20 show the likely performance of the HLL and HLLC solvers for contacts, shear waves and vortices. Speci cally the gure shows the results for an isolated contact wave, where the HLLC pres3(T)ats47T -32.21g wa0oetTofHLL solve(.)-429(The)]TJ 0 -17
wherats the HLLCh(a)28(v)27(es)-484(exaclly)-428(ts)-486(the)-428(exact)-429(Riemann)-428(solv)28(eL)-428(fo
chemevts nitesresolutionfor stationary contact wavtsandthedisipautionfor

7.3 Osher

The Osher-Solomon scheme proved to be very elaborate to code. Despite numerous attempts to produce a working scheme in FORTRAN-95, we could not escape wild uctuations at the discontinuities. The scheme, like others, was aimed to be subject to several tests, presented in Table 7.3.

Test	$_L$	u_L	p_L	$_R$	u_R	p_R
1	1.0	0.75	1.0	0.125	0.0	0.1
2	1.0	-2.0	0.4	1.0	2.0	0.4
3	1.0	0.0	1000.0	1.0	0.0	0.01
4	5.99924	19.5975	460.894	5.99242	-6.19633	46.0950
5	1.0	-19.59745	1000.0	1.0	-19.59745	0.01
6	1.0	2.0	0.1	1.0	-2.0	0.1

Table 7.3: Data for ve Riemann problem tests

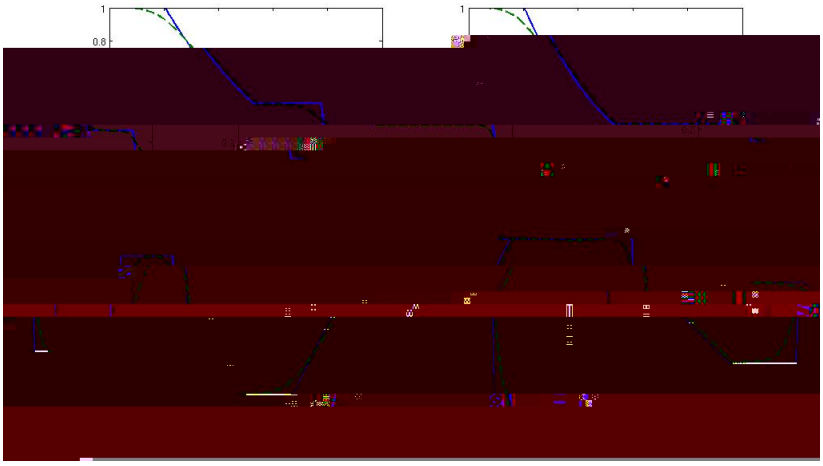

Figure 7.21: Osher Riemann solver applied to Test 1 of Table 7.3, with P-ordering. Numerical (dash) and exact (line) solutions compared at time 0.2

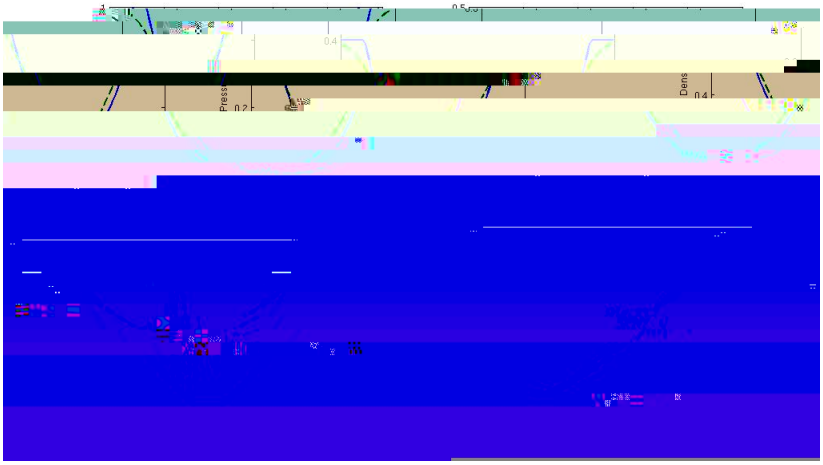

Figure 7.22: Osher-Solomon Riemann solver applied to test 2 of Table 7.3, with P-ordering. Numerical (dash) and exact (line) solutions compared at time 0.15

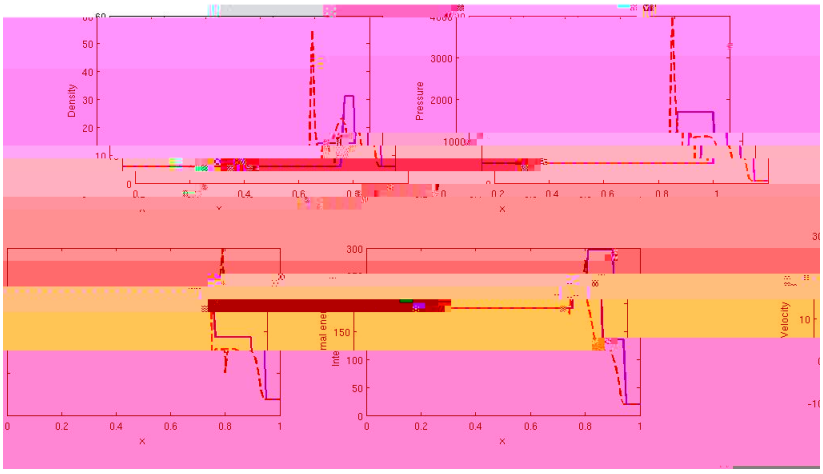

Figure 7.23: Osher-Solomon Riemann solver applied to test 4 of Table 7.3, with P-ordering. Numerical (dash) and exact (line) solutions compared at time 0.012

7.4 The tests

Here we use the tests originally presented in Section 2.3. We recap on these tests in Table 7.4

Test	$_L$	u_L	p_L	$_R$	u_R	p_R
1	1.0	0.0	1.0	0.125	0.0	0.1
2	1.0	-2.0	0.4	1.0	2.0	0.4
3	1.0	0.0	1000.0	1.0	0.0	0.01
4	1.0	0.0	0.01	1.0	0.0	100.0
5	5.99924	19.5975	460.894	5.99242	-6.19633	46.0950

Table 7.4: Data for ve Riemann problem tests

While we used modi ed versions of these for each solver, we now use the unmodi ed versions on all schemes, with the exception of the Osher-Solomon scheme, for comparison.

7.4.1 Test 1

Test 1 is the mildest test, and is known as the Sod test problem.It consists of a left rarefaction, a contact and a right shock. Pro les were taken at time $t = 0.25$ and initial position $x_0 = 0.5$. All schemes are adept at handling this problem.

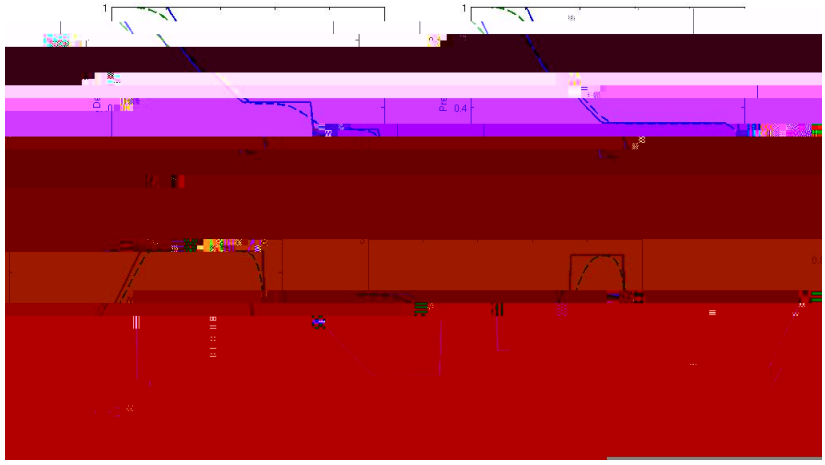

Figure 7.24: HLL Riemann solver applied to test 1 of Table 7.4, with Einfeldt wave speed. Numerical (dash) and exact (line) solutions compared at time 0.25

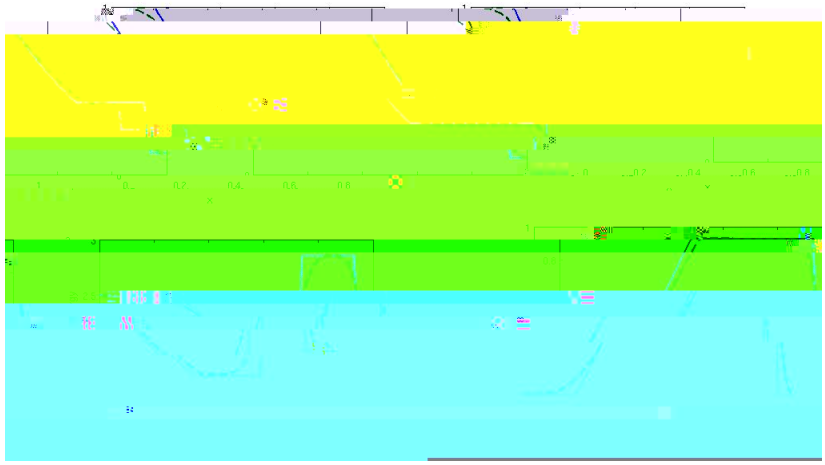

Figure 7.25: HLLC Riemann solver applied to test 1 of Table 7.4. Numerical (dash) and exact (line) solutions compared at time 0.25

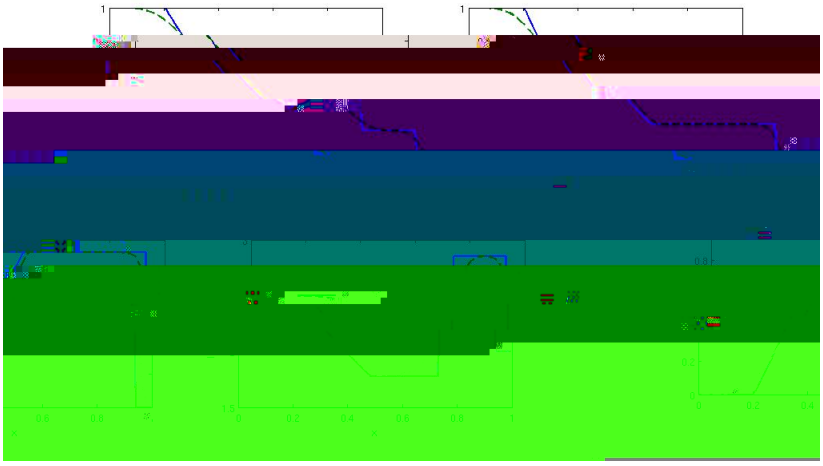

Figure 7.26: Roe Riemann solver applied to test 1 of Table 7.4. Numerical (dash) and exact (line) solutions compared at time 0.25

7.4.2 Test 2

Test 2 is otherwise known as the *123 problem*. Consisting of two strong rarefactions and a trivial stationary contact discontinuity. Pro les were taken at time t = 0:15 and initial position x_0 = 0:5. The HLL scheme did not produce su cient results to enable plotting of a graph, with the scheme breaking down early. One of the most notable points is that none of the schemes very su ciently give accurate results for the speci c internal energy.

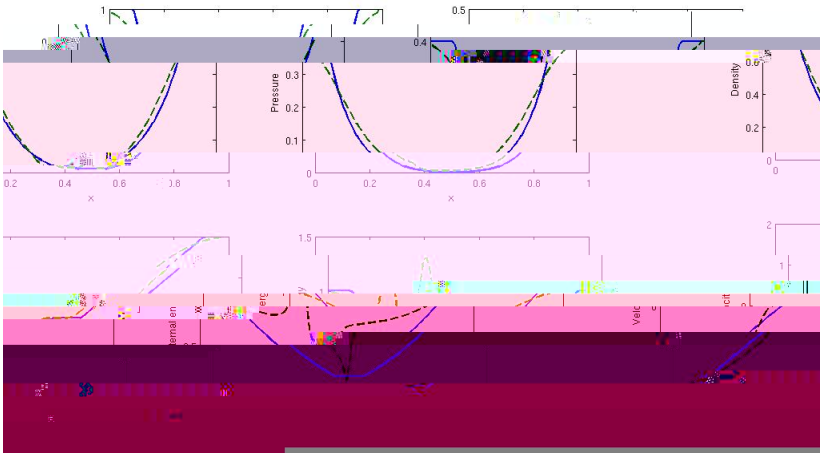

Figure 7.27: HLLC Riemann solver applied to test 2 of Table 7.4. Numerical (dash) and exact (line) solutions compared at time 0.15

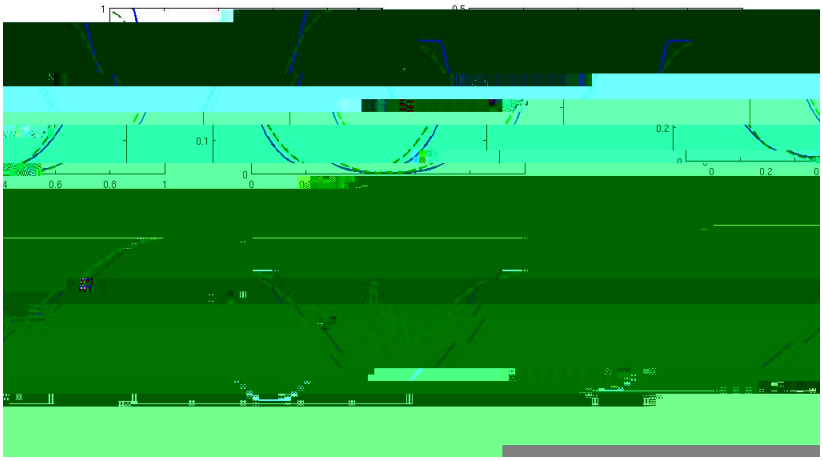

Figure 7.28: Roe Riemann solver applied to test 2 of Table 7.4. Numerical (dash) and exact (line) solutions compared at time 0.15

7.4.3 Test 3

Test 3 represents the left-hand side of the blast wave problem.

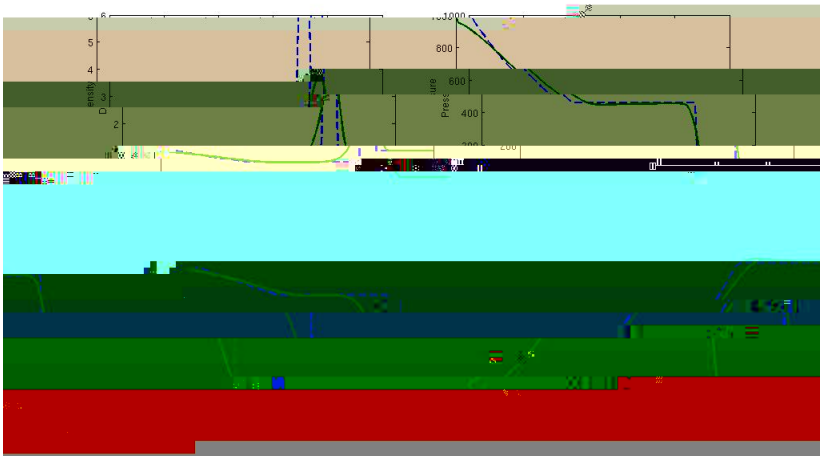

Figure 7.29: HLL Riemann solver applied to test 3 of Table 7.4. Numerical (dash) and exact (line) solutions compared at time 0.012

7.4.4 Test 5

Recall that test 5 is made up from right and left shocks emerging from the solution of the blast wave problem of tests 3 and 4. The solution of test 5 represents the collision of two strong shocks and consists of a left facing shock travelling slowly right, a right travelling contact discontinuity and a right travelling shock wave [20]. Pro les were taken at time t = 0:012 and initial position x_0 = 0:8.

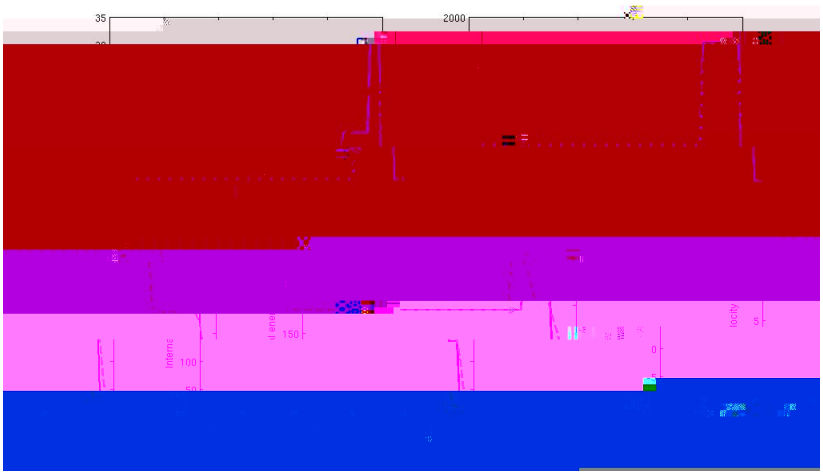

Figure 7.32: HLL Riemann solver applied to test 5 of Table 7.4, with Einfeldt wave speed. Numerical (dash) and exact (line) solutions compared at time 0.012

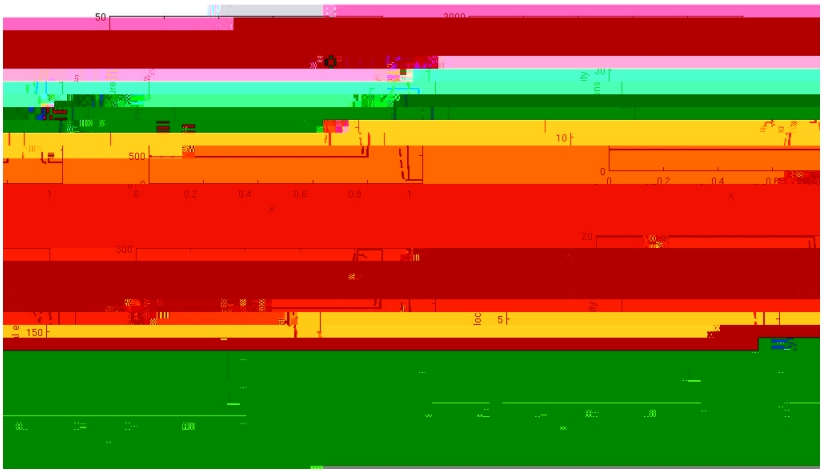

Figure 7.33: HLLC Riemann solver applied to test 5 of Table 7.4. Numerical (dash) and exact (line) solutions compared at time 0.012

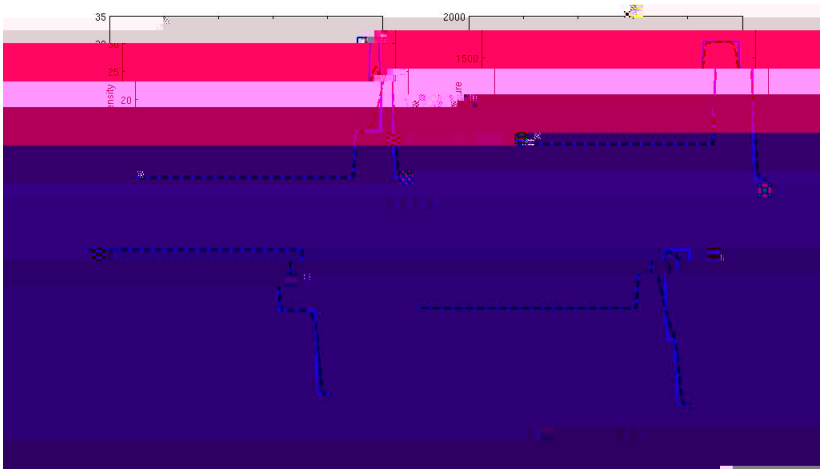

Figure 7.34: Roe Riemann solver applied to test 5 of Table 7.4. Numerical (dash) and exact (line) solutions compared at time 0.012

7.5 Second Order Results

It is desirable to produce higher order results for the schemes as this signi cantly improves the accuracy. In this section the results of the method described in Section 6 as applied to the Riemann solver of Roe are presented. Each test was performed using Sod's shock tube (2.8), with the discontinuity at x_0 = 0:5 to demonstrate how much more accurate the scheme is at second order. For all tests the one-dimensional time dependent Euler equations were used as ideal agses with = 1:4. The exact and numerical solutions are found in the spatial domain 0 x 1. The numerical solutions are computed with M = 100 and the CFL is 0.5.

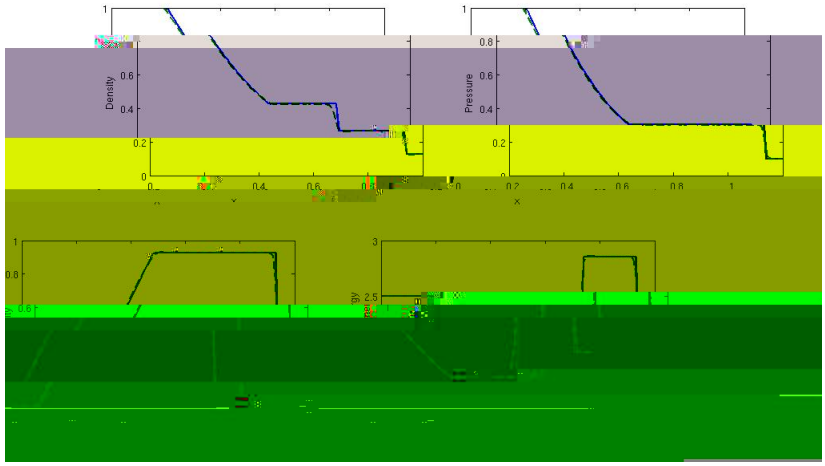

Figure 7.35: Flux Limiter Scheme for second order with Roe Riemann solver and Superbee applied to Sod's shock tube problem (refeq:sod). Numerical (dash) and exact (line) solutions at time t= 0.25

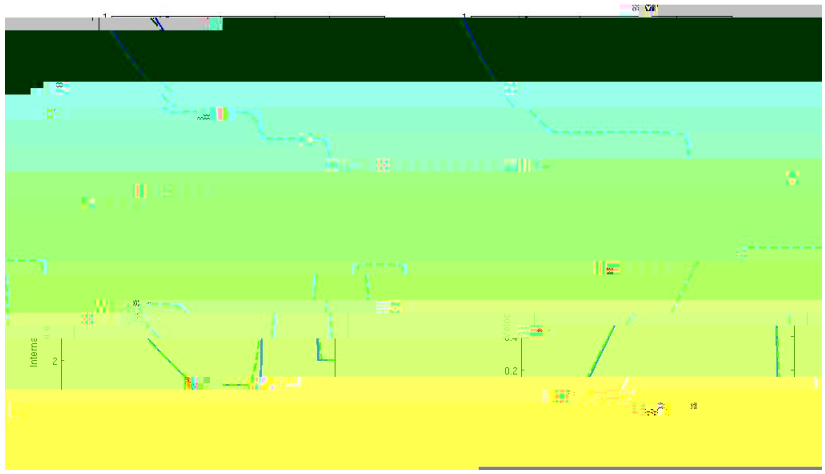

Figure 7.36: Flux Limiter Scheme for second order with Roe Riemann solver and van Leer applied to Sod's shock tube problem (refeq:sod). Numerical (dash) and exact (line) solutions at time t= 0.25

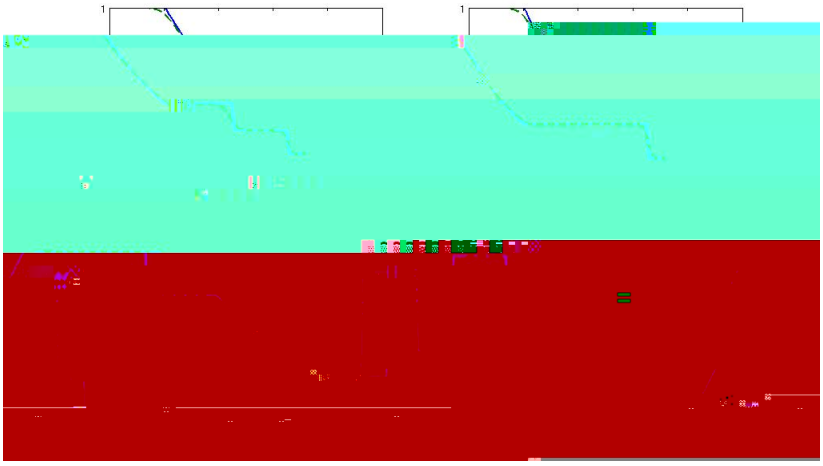

Figure 7.37: Flux Limiter Scheme for second order with Roe Riemann solver and Minmod applied to Sod's shock

8 Discussion

This section aims to clarify what is shown in the results section and expand on how the study can be further improved. We will look at the results given in Section 7 separately and hollistically to compare and contrast the various Riemann solvers presented. We will also discuss how these tests may be extended and improved upon for future study.

To rst consider the Roe Riemann solver and the tests performed in Section 7.1, we have found some notable faults in the scheme. One fault is that Test 2 showed the failure of the scheme near

One of the most unfortunate parts of this study was the failure to reach a working code for the Osher-Solomon scheme. Perhaps, if nothing else, this demonstrates how impratical the scheme is, as the large tables of comparison to choose u_x lead to computational and time expense. In order to evaluate u_x any code must work through 16 cases for the one-dimensional Euler case. In fact, it is

could then be tested, leading to some very interesting three-dimensional models with perhaps more pratical implications. Reviews of higher-order and multi-dimensional methods can be found in comprehensive texts such as LeVeque [8] and Toro [20].

9 Conclusion

In this paper, we have presented three high-resolution schemes and applied them to approximate Euler equations. Several test cases were used to test the numerical schemes and highlight their strengths and weaknesses. We highlighted how Roe's scheme performed well, however it failed at low-density ows. Overall it was shown to be a robust scheme, performing to exact standards at second order. We then showed how the simple HLL scheme produced good results, a very desirable scheme due to the simplicity-to-accuracy ratio, however it lacked accuracy at some forms of contact discontinuities. We then showed how the HLLC scheme improved on this, however due to some errors we were unable to demonstrate some of its desirable properties and it su ered more di usion than Roe's scheme. We then looked at the Osher-Solomon scheme, a very expensive and complex

10 Bibliography

References

[1]

[14] Rusanov, V. Calculation of interaction of non-steady shock waves with obstacles. *J. Comput. Math. Phys. USSR 1* (1961), 267{279.

[15] Sod, G. A survey of several nite di erence methods for systems of nonlinear hyperbolic conservation laws. *J. Comp. Phys. 27* (1978), 1{31.

[16] Sweby, P. Exact riemann solver. University of Reading, UK, 2011.

[17] Toro, E. A linearised riemann solver for the time-dependent euler equations of gas dynamics. *Proc. Roy. Soc. London A434* (1991), 683{693.

[18] Toro, E. On glimm-related schemes for conservation laws. Technical Report 97-02, Department of Mathematics and Physics, Manchester Metropolitan University, UK, 1997.

[19] Toro, E., Spruce, M., and Speares, W. Restoration of the contact surface in the hll-riemann solver. *Shock Waves 4* (1994), 25{34.

[20] Toto, E. *Riemann Solvers and Numerical Methods for Fluid Dynamics: A Pratical Introduction*. Springer, UK, 1999.

[21] van Leer, B. Towards the ultimate conservative di erence scheme ii: Monotonicity and conservation combined in a second order scheme. *J. Comp. Phys. 14* (1974), 361{370.

[22] Woodward, P., and Colella, P. The numerical simulation of two-dimensional uid ow with strong shocks. *J. Comput. Phys. 54* (1984), 115{173.